

Двофазне впорскування рідкого газу являє собою важливий промисловий процес, який використовується в більшості сепараторів. На ранній стадії впорскування утворюється циліндрична бульбашка. З плином часу форма бульбашки стає все більш складною і дуже важкою для аналізу. В даному дослідженні розроблена проста аналітична модель для пояснення зміни форми бульбашки. Аналітична модель була розроблена на основі інерції потоку води, який безперервно штовхає бульбашку, в той час як сила опору чинить опір йому, так що лобова площа бульбашки збільшується. Розмір бульбашки і її лобову площу оцінювали з використанням припущення про рівновагу між силою інерції і силою опору, нехтуючи в'язкою силою. Виходячи з оцінки, можна визначити роль вихрового кільця по різниці теоретичних і експериментальних результатів. Аналітичну модель перевіряли за допомогою зібраних експериментальних даних по деформації форми, викликаної рухом бульбашки на початку впорскування. Експериментальні дані, використані в якості перевірки, вимірювали по зображенню носа бульбашки з десятикратним повторенням з похибкою  $\pm 6\%$ . Експериментальний метод проводиться шляхом уприскування бульбашки в горизонтальному напрямку в басейн з водою. Інерційна сила потоку води перед носом бульбашки створює бульбашку. Бульбашка раптово змінює свою форму, рухається у вигляді бульбашкового струменя і зазнає поступові зміни форми. Лобова площа бульбашки збільшується і досягає максимуму в кінцевій точці швидкості. На деформацію форми бульбашки впливає інерційна сила потоку води, яка штовхає бульбашку вперед. Відповідно, бульбашка змінює свою форму з циліндричної на сферичну, а потім на еліпсоїдальний диск. По досягненню бульбашкою граничної швидкості, сила інерції стає рівною силі опору. Край бульбашки у вигляді еліпсоїдального диска демонструє підвищений поверхневий натяг. Різниця між експериментальними даними та аналітичною моделлю обумовлена складним текучим і динамічним потоком, оточуючим бульбашку. Передбачається, що математична база, запропонована в даній роботі, стане важливим інструментом для прогнозування лобової площі бульбашки

**Ключові слова:** *впорскування, деформація, форма бульбашки, лобова площа*

UDC 532.529

DOI: 10.15587/1729-4061.2020.204102

# EXPERIMENTAL AND THEORETICAL BUBBLE GROWTH COMPARISON AT THE INITIAL STAGES OF HORIZONTAL INJECTION

Tri Tjahjono

Doctoral Student in Mechanical Engineering\*

Lecturer

Department of Mechanical Engineering

Faculty of Engineering

Universitas Muhammadiyah Surakarta

Jl. A. Yani Tromol Pos 1, Pabelan, Kartasura,

Surakarta 57102, Indonesia

E-mail: tri.tjahjono@ums.ac.id

I. N. Gede Wardana

Professor in Mechanical Engineering\*

E-mail: wardana@ub.ac.id

Mega Nur Sasongko

Associate Professor in Mechanical Engineering\*

E-mail: megasasongko@ub.ac.id

Agung Sugeng Widodo

Associate Professor in Mechanical Engineering\*

E-mail: agung\_sw@ub.ac.id

\*Department of Mechanical Engineering

Brawijaya University

Jl. Mayjen Haryono, 167, Malang, Indonesia, 65145

Received date 20.03.2020

Accepted date 22.05.2020

Published date 19.06.2020

Copyright © 2020, Tri Tjahjono, I. N. Gede Wardana, Mega Nur Sasongko, Agung Sugeng Widodo

This is an open access article under the CC BY license

<http://creativecommons.org/licenses/by/4.0>

## 1. Introduction

In the cases of two-phase flow, such as those encountered in a gas separator, particularly in liquid-gas interfaces, not all the gases can be separated mechanically during injection. One of the problems in the two-phase flow, which occurs during the horizontal injection through stagnant liquids, such as water, is attributed to the behavior of the bubble, which is related to the operational performance of the injector. The restriction force of a bubble in a two-phase flow system is not constant compared to that generated in a solid body. The frontal area of the bubble can be developed up to a maximum at the terminal velocity. This obstructs the bubble separation process. The restriction force of the bubble in the water flow is influenced by the shape of the bubble. The different forms of bubble deformation around the interface between the bubble surface and the water depend on the hydrodynamic forces that are associated with the patterns of liquid flow [1].

The existence of bubble growth will affect the flow pattern around the bubble. So this flow pattern influences each other. Bubble growth and changes in flow patterns will decrease the speed of the two-phase injection flow. The decrease of injection speed will reduce the magnitude of centrifugal force in the cyclonic separator. The function of centrifugal force is a separation between bubbles and water in the separator. The separation process of the bubbles in the cyclone separator does not give satisfactory results, namely the bubbles that still follow with the water flow. For this reason, research is needed to obtain operational improvement.

## 2. Literature review and problem statement

The paper [2] presents the results of research about experimental and theoretical study that focuses on the hydrodynamic flow behaviour applied in a Gas-Liquid Cylindrical

Cyclone (GLCC) compact separator. Works on GLCC have succeeded in field application, which has a real impact on technology for the industry. It is shown that the tangential inlet of injection gives a swirling motion and makes the gas and liquid phases separated by the centrifugal and gravitational forces. The liquid mass is higher than gas, which is impelled to the cylinder wall and flows down by gravity, while the gas is forced towards the center of the cyclone and moves up. But there were unresolved issues related to the lack of models and data and a little understanding of hydrodynamic flow behavior in the GLCC and needed further research and development. The reason for this may be understanding about the flow behavior in the GLCC that will help the development of the GLCC as an attractive choice than the conventional separator. In the injection operation, the bubble content will be influenced by many factors, for example, fluid characteristics and properties; operation conditions (flow capacities, pressure and operation temperature of fluid); diameter and position of the nozzle. In the flow physics, current understanding for detailed phase separation and interaction during the operation is still very limited, and it is even worse for operation at the off-design condition that could have a significant influence on the nominal performance of flow injection. A way to overcome these difficulties can be investigating a part of many causes of the problems. The method used requires a simpler research to look for causes and effects, which is then further refined. This approach was used in [3], however, the program was performed in several tests for the phase separation and flow hydrodynamic processes. This work explains the principles of the operational cyclone separator by revealing laboratory and field data and gives the modelling foundations. The laboratory tests were conducted in simple models operating with mixtures of air and water. All this suggests that it is advisable to conduct a study on technology for offshore operations that is very costly, especially for the required size and weight, strong structures are needed. To exploit offshore oil reserves, it is needed to reduce equipment costs, inspiring the new research by improving gas-liquid separation techniques.

This study aimed to investigate the behavior of a bubble when it is initially injected along the horizontal direction in stagnant water. The specific sub-aims are to:

- study the effects of fluid flow on the shape of the bubble;
- mathematically model the changes of the bubble shape related to the frontal area that affects the efficiency of the bubble separation;
- identify the terminal velocity point or the maximum frontal area.

The behavior of a single bubble in terms of liquid phase properties and bubble sizes has been studied previously [4]. The velocity of a bubble moving in a liquid depends on a number of factors, such as the bubble size, the interfacial tension, and the viscosity and density of the liquid [5]. Therefore, the velocity and shape of a single bubble are interrelated. Studies have also been conducted on shape deformations and aspect ratios of the bubbles injected in the upward direction from the initial injection phase to the stage at which the bubble attained its terminal velocity [6]. It has been shown in many experiments that the force of gravity, buoyancy, and momentum of water flow affect the shape of the bubble [5, 7]. Accordingly, the effects of the pressure field on the growth of the bubble and on the deformation of its shape post-injection have been investigated [7].

Another study was also conducted to assess the accuracy of the length of void penetration in blowdown pipes that were submerged in water to force the gas in the containment pool, similar to the case of a gas line [8]. Research was also conducted to study the formation of the bubble following gas injection into turbulent, downward-flowing water, through a submerged pipe in a water pond [9]. It was found that during the early steps of injection, the diameter of the pipe affected the bubble size. The bubble size increased as the gas-injection flow rate increased and as the liquid velocity in the downward flow decreased. A study was carried out to characterize the parameters of the gas-liquid interface within a downward jet in a circular bubble column [10]. It was found that the interfacial area had a profound influence on the slip velocity of the bubble. When a bubble is pushed by the inertial force exerted at its tail, it deforms from its original spherical shape to attain an ellipsoidal disk shape [11]. The bubble shape is controlled by the surface tension and the inertial force of the bubble in water. The viscous force has a small influence on the bubble shape, which is normally ignored [12]. The bubble undergoes changes in shape that are influenced by the pattern of the fluid flow around it [13]. At the bubble nose, the bubble surface changes from a flat to a convex form within a short time period. Correspondingly, the end-part of the bubble, which is sharp, has a higher surface energy. The effect of the inertial force or kinetic energy in the end-part is delivered to other parts, which have lower energies. The neck form of the bubble surface indicates the onset of the bubble breakup. This is analogous to the increase of the surface energy density of a droplet fragment compared to that of the original bubble before breakup [14].

A recent study reported that a vortex ring travels at the inlet beat velocity, rolls up, and is then transmitted downstream to form a shear layer [15]. If the layer contacts the bubble surface, it can change the shape of the bubble. The nature of the vortex ring is established by considering the intensity of the kinetic energy, the momentum, and the movement of the vortex ring from the circling jet into the primary vortex ring [16]. After the bubble is in contact with the vortex ring, the bubble continues to pinch-off. This is a fast process, which occurs near the breakup point. The breakup of the air bubble has been observed in submerged nozzles in different liquids [17].

The significance of this research work is attributed to the fact that it can predict the energy absorbed by the bubble, as evidenced by the physical appearance of the bubble. From the onset of the injection flow to the instant at which the terminal velocity is attained, the bubble deformation occurs gradually. This means that there is an energy change from kinetic to surface. From the first to the last points of bubble movements (terminal velocity state), there are equilibrium forces between the inertial and the drag forces [18]. The drag force occurs in the frontal area and can restrict the liquid flow. In a cyclonic separator device, this is very disturbing because of the decreased centrifugal force.

Another study was conducted to evaluate the bubble flow injection vertically in quiescent water [6]. An air bubble was detached from the nozzle at the first step. The kinetic energy of the bubble was used to overcome the drag and the fluid viscosity, which deformed the bubble shape from a bullet to a spherical shape. At the second step, the spherical bubble changed to an ellipsoidal form as the kinetic energy transformed to surface energy based on the increase of the bubble surface area [19].

Many researchers studied the bubble flow injection based on upward and downward modes. The bubbles were subjected to gravitational force. In this research, a bubble was horizontally injected through stagnant water without the influences of gravitational forces. In the upward and downward flow injections, the bubble drag was affected by the buoyancy and gravity forces. However, in horizontal flow injection cases, it was only affected by the inertial force. The bubbles were injected into a turbulent flow of liquid along a horizontal line [20]. In this research, a bubble was horizontally injected in a stagnant water bath. A mathematical formulation can be used as a basic reference for the prediction of the frontal area based on the restriction of the flow velocity of injection. The bubble injection process during a transient stage can provide insights for an improved design of the separation device.

Bubble separation process in a cyclone separator is difficult to predict because of many factors, one of them is hydrodynamic flow patterns [3]. This simple research tries to investigate flow injection of a bubble in stagnant water. By investigating bubble behaviour, two-phase flow injection gets a flow pattern that can influence bubble movement and bubble size. Measurement of bubble size is needed for the indication of bubble change. Bubble shape always changes, so the flow pattern is difficult to determine. At least the main flow patterns can be known.

In the injection process, the bubble size is increased and then the decrease in its size at certain time occurs, between the interval sizes there is a peak point. This point indicates a maximum size of the frontal area. This area has a diameter, which is important taken part in the mathematical model.

Drag force is proportional to the frontal area in the water injection. If the water flow velocity decreases, this is followed by increasing frontal area. This area continues to increase starting from the outlet nozzle up to the early decrease in its size. Finally, the terminal velocity point can be determined before a decrease of the bubble size.

### 3. The aim and objectives of the study

The aim of the study is an investigation of the performance of the bubble separation process in the cyclone separator, which does not provide satisfactory results. This study needs to do a simple injected model to obtain information on the behavior of the hydrodynamic mechanism for operational improvement.

To achieve this aim, the following objectives are accomplished:

- calculating the maximum growth of bubbles is achieved by a mathematical approach. To compare this prediction it is important to trace the bubble growth experimentally;
- measuring a bubble size from the exit nozzle to the following terminal point is to indicate the change of the frontal area at initial injection. How large is the frontal area that can be achieved;
- comparing theoretical and experimental changes to predict the cause of bubble changes.

### 4. Research work methodology

#### 4. 1. Theoretical model

When a bubble exits from the outlet of the nozzle through the static water in a cylinder, the inertial force,  $F_i$ ,

which acts on the bubble will be counterbalanced by a drag force,  $F_D$ , and by a viscous force,  $F_V$ , as expressed by eq. (1):

$$F_i = F_V + F_D, \tag{1}$$

During the bubble travel, an increase of  $F_D$  will be followed by a decrease of  $F_V$ . The radius of the sphere geometry, which is initially the same as that of the cylinder core, increases and causes the bubble to expand if the surrounding pressure is uniform, as shown in Fig. 1.

The magnitude of the viscous force of the sphere is smaller than that of the cylindrical form because of the decrease of the shearing surface area. When the momentum or inertial force of the water flow is continually applied to the sphere, its shape changes to an ellipsoidal disk, as shown in Fig. 2, with  $a$ ,  $b$ , and  $c$  being the radii of the core with respect to the  $x$ ,  $y$ , and  $z$  axes, respectively. Consequently, the drag force increases to a maximum value, and the viscous force decreases to a minimum value, and even approaches zero. This is in accordance with the studies of the terminal velocity of single bubbles [6] and has also been discussed on the shape and motion of air bubbles [12], which stated that the viscous force is much smaller than the inertial and surface (or drag) forces.

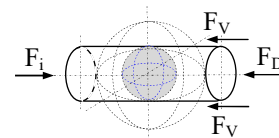


Fig. 1. Change in the bubble shape from cylindrical to spherical forms

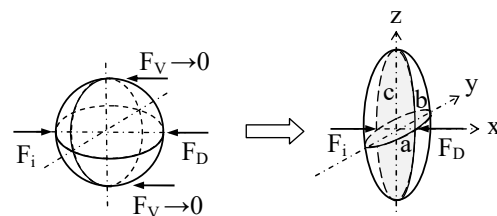


Fig. 2. Change in the bubble shape from a spherical to an ellipsoidal disk form

When the viscous force reduces to zero, the shearing surface area approaches zero, and the frontal area (drag area) increases. Accordingly, eq. (1) can be rewritten as:

$$F_i = F_D, \tag{2}$$

Because the inertial force on the back side of the bubble ( $x$ -axis direction) is continually exerted on the spherical bubble, the shape of the bubble changes to an ellipsoidal disk. The change in the position vector in the  $y$  direction is assumed to be the same as that along the  $z$  direction because a) the bubble shape is small or b) because the water depth in the case of the bubble that is very small becomes similar to the bubble radius. The difference of the static pressures on the bubble surface on the  $y$  and  $z$  axes is not significant.

When the terminal velocity is achieved in the case of horizontal bubble flow, there is no change in the frontal area of the bubble. A fraction of the kinetic energy of the flow is transferred to the surface bubble energy. The density of the surface energy on the edge of the ellipsoidal disk of the bubble increases to its maximum value.

Based on eq. (2), whereby  $F_i$  is equal to  $F_D$ , the bubble velocity  $v$  can be expressed as a function of the drag coefficient,  $C_D$ , time,  $t$ , and bubble radius,  $r_x$ :

$$v = \frac{8r_x}{3C_D \cdot t} \tag{3}$$

From eq. (3), decreasing the radius  $r_x$  in the  $x$  direction results in an increase in the frontal area of the bubble.

Bubbles rise through a stagnant liquid owing to gravity and buoyancy forces. In contrast, the bubble motion in horizontal flow injection cases is influenced by the force of the liquid flow. Thus, the gravity and buoyancy forces on the vertically moving bubble can be analogous to the momentum on the horizontally moving bubble. If the form of the vertical moving bubble is similar to the form of the horizontally moving bubble, the  $C_D$  formulation of eq. (4) can be adopted. The model for the drag coefficient  $C_D$  depends on the Reynolds number  $Re$  of the deformed bubble, such as the case of the ellipsoidal bubble [21, 22]

$$C_D = \frac{48}{Re} \left( 1 - \frac{2.21}{\sqrt{Re}} \right) \tag{4}$$

It should be noted that the bubble width decreases after the bubble exits from the outlet of the nozzle up to the instant at which the terminal velocity is attained. Coincidentally, the frontal area of the bubble starts to expand in any radial direction. As the bubble shape changes to an ellipsoidal, the spherical radii of  $a$  decrease. The reduction of  $a$  is followed by the increase in  $b$  and  $c$ . As the magnitude of  $b$  is the same as that of  $c$ , the formula of the ellipsoidal disk is given by:

$$\frac{x^2}{a^2} + \frac{y^2 + z^2}{b^2} = 1 \tag{5}$$

The changes of the radius, which are affected by the inertial force can be analyzed according to the position vector (Fig. 3).

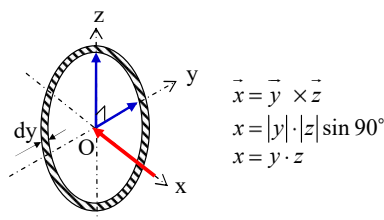


Fig. 3. Vector of momentum along the negative  $x$  direction is radially distributed in the frontal  $y$ - $z$  plane

Because the size of the bubble is very small, it can be assumed that the difference in water depth between its top and its bottom is not significant. As the bubble shape becomes ellipsoidal, the frontal area in the  $x$  direction has a circular form. The increment of the ellipsoidal disk radius in the  $x$  direction is the same as those in radial directions ( $y$  and  $z$  directions of the Cartesian coordinate system), as formulated in eq. (6):

$$\mathbf{x} = \mathbf{z} \cdot \mathbf{z} = \mathbf{z}^2, \tag{6}$$

where  $\mathbf{x}$  is the vector area of the quadrangular, and  $\mathbf{z}$  is the vector radius of the spherical bubble. Fig. 4,  $a$  shows the

change in the bubble shape due to the changes of the radii in the  $x$ ,  $y$ , and  $z$  directions. The size of the bubble decreases in the  $x$  direction and increases in the  $y$  and  $z$  directions. Fig. 4,  $b$  shows that the enlarged spread of the bubble frontal area in the radial directions is a function of time  $t$  because the water flow continually pushes on it. This means that the linear momentum change in the  $x$  direction is converted to the quadratic function of the frontal area in the  $y$  and  $z$  directions. The incremental changes of the radii in (6) are then adapted using the derivation formulated in (7):

$$dz = \frac{1}{2}x^{-1/2}dx \tag{7}$$

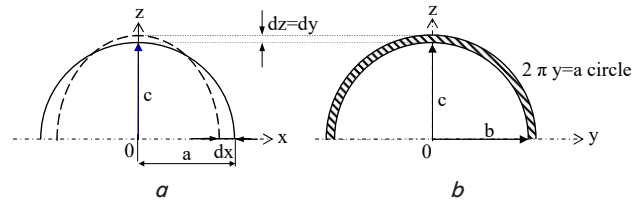


Fig. 4. Bubble deformation:  
 $a$  – change in the  $x$ - $z$  plane;  
 $b$  – change in the frontal area in the  $y$ - $z$  plane

The frontal area of the bubble can be determined from eq. (5). As the change in the frontal area is a function of time, eq. (5) is required to be re-expressed as a function of  $t$ :

$$2y^2 = b^2 - \frac{b^2}{a^2}x^2, \tag{8}$$

$$4ydy = -\frac{b^2}{a^2}2xdx, \tag{9}$$

where from eq. 3, if  $r_x$  as a radius of  $a$ :

$$a = \frac{3}{8}C_D vt. \tag{10}$$

To find the change in the frontal area ( $A_{ch}$ ), both sides of (9) are multiplied by  $\pi/2$  and are then integrated.

$$\begin{aligned} A_{ch} &= \int_{y_0=b}^{y_n=b_n} 2\pi y dy = -\frac{b^2}{2a^2} \pi \int_{x_0=a}^{x_n=a_n} 2x dx = \\ &= -\frac{b^2}{a^2} \pi \left[ \frac{x^2}{2} \right]_a^{a_n}, \\ A_{ch} &= \frac{\pi b^2}{2a^2} (a^2 - a_n^2), \end{aligned} \tag{11}$$

where  $n$  is the time order (1, 2, 3, ...).

#### 4. 2. Experimental setup

The experiment was carried out in a rectangular tub, which was filled with water. The dimensions of the water tub in static conditions were 1000 mm (length), 200 mm (width), and 200 mm (height) (Fig. 5).

A hole was created at a depth of 100 mm in one of the tub sides as a syringe drain outlet. The bubble was prepared manually with a pipette with an extended small flexible pipe inserted into the syringe line. The nozzle of the syringe line had an inner diameter of 1.5 mm. When the syringe was

pressed, a bubble was created within the water inside the syringe line. The bubble then arose from the syringe line to the water in the tub. As the bubble entered the tub, the surface level of the water was increased. However, the water surface in the tub was maintained with the use of water overflow. This method was adopted to maintain the static pressure on the bubble immediately after its injection from the nozzle along the horizontal direction.

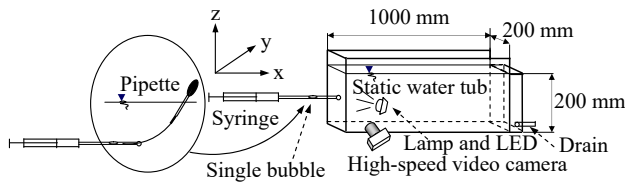


Fig. 5. Bubble flow injection test bed (LED: light emitting diode)

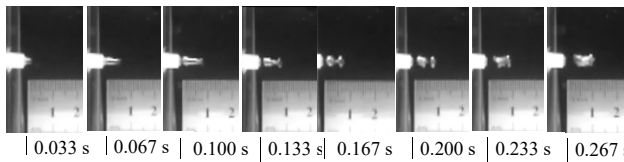


Fig. 6. Bubble formation at the initial injection phase

Fig. 6 shows the bubble exiting from the nozzle at the initial injection stage. To obtain the two-dimensional image of the bubble path line, the bubble images were captured by a high-speed digital camera (Fuji Film Finepix HS55EXR) at the rate of 480 frames per second. At this rate, the number of pixels in one frame was equal to 320×112.

### 5. Results and comparison between the theoretical and experimental theory

Fig. 7 illustrates the temporal variation of the bubble velocity obtained theoretically and experimentally. The dashed line plot is the theoretically estimated bubble velocity, while the solid line plot is that obtained experimentally. The trend of theoretical velocity evolution agrees very well with the experimental results for  $t > 0.1$  s. The increased similarity of the experimental data after 0.20 s is attributed to the induction of the inertial force of the water flow in front of the bubble nose. However, for  $t < 0.1$  s, the velocity difference between theory and experiment is very large, which may be attributed to the discharge loss effect on the outlet nozzle [23].

The change in the bubble shape observed experimentally is shown in Fig. 8. The result indicates that the shape of the bubble increases along the z-axis and decreases along the x-axis, thus indicating that the bubble surface is flattened. The formation of the flat bubble is evidence for the development of a frontal bubble area. An increase in the bubble frontal area enhances the drag force of the bubble, which can restrict the water flow. The analysis of one bubble can be used to predict the behavior of a number of bubbles generated in the two-phase flow system, which would induce a larger drag force. Therefore, the drag force cannot be ignored in the study of the physical characteristics of the bubble. When the bubbles coalesce, the drag force will increase, which will restrict the water flow. In a cyclonic separator, the increase of the drag force would decrease the centrifugal force, which results in

the decrease of the bubble separation. In contrast, if the bubbles break up into very small sizes, the bubble content in the fluid flow becomes difficult to separate. Bubble separation is based on the principle of buoyancy force – small bubbles have a buoyancy force smaller than the inertia force of fluid flow, with which these small bubbles tend to induce the flow.

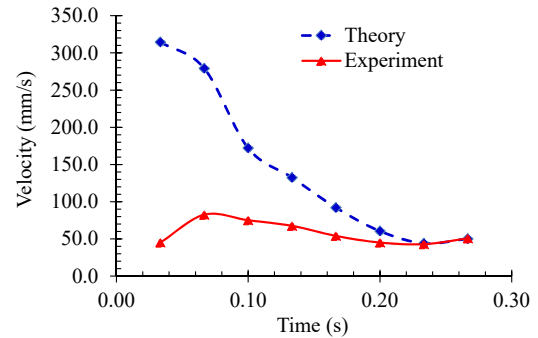


Fig. 7. Theoretical and experimental velocity (mm/s) profiles of a bubble

In Fig. 7, the velocity of experimental data was estimated from the video image movie presented in Fig. 6. The uncertainty of the velocity of experimental data was  $\pm 6\%$ . It can be seen that the velocity data of the experiment are lower than the velocity of theoretical analysis at the initial part that means any losses at the exit nozzle and water drag along a bubble flow. The end part shows relatively the same value, because experiment and theory velocities are only effected drag.

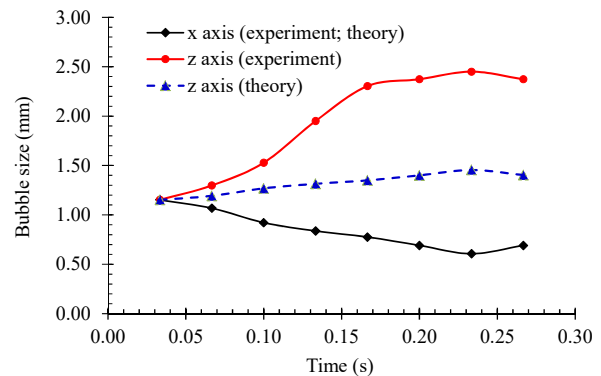


Fig. 8. Temporal variations of bubble shape in the  $x$  and  $y$  axes. Theoretical and experimental values of the  $x$ -axis (black line) are considered equal in computing the difference between the experimental  $z$ -axis value (red line) and theoretical  $z$ -axis value (blue line)

The difference of bubble height ( $z$  axis) between experiment and theory indicates the vortex ring plays a role in the bubble shape. Bubble size gets an increase in the  $z$  axis along the vortex contributes force on the bubble.

A spherical form deforms to an ellipsoid disk form, in theory causes of its transformation can be predicted. If any difference between experiment and theory, there are other causes of what is analyzed in theory.

Change of bubble shape from a sphere to an ellipsoid causes the frontal area to increase. Frontal area difference between experimental and theoretical influences each other hydrodynamic behavior and bubble shape. Frontal area change is correlation with restriction of hydrodynamic flow.

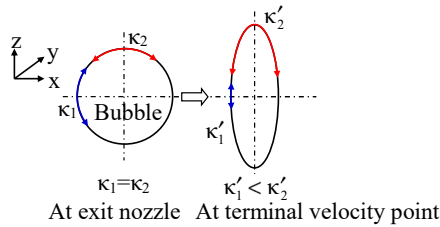


Fig. 9. Bubble deformation from a spherical form to an ellipsoid disk form

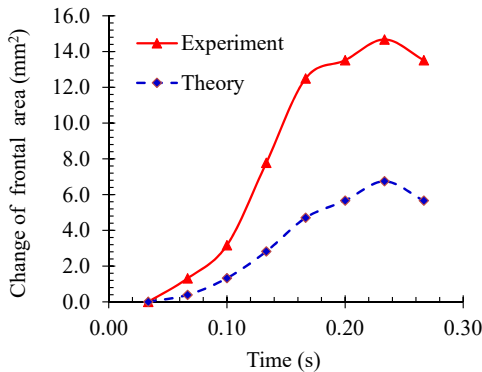


Fig. 10. Theoretical and experimental changes of the frontal areas of a bubble

### 6. Discussion of experimental results

The inertial force of the injection flow changes the bubble shape from spherical to ellipsoid. Fig. 9 shows the reduction of the bubble size in the  $x$  direction, which causes the bubble elongation in the  $z$  direction. The diameter differences of the  $x$  and  $z$  directions indicate the presence of the surface stress ( $\sigma$ ) and the curve factor ( $\kappa$ ) change in the bubble. As the liquid pressure increases, the surface stress is increased at the bubble tail. Because the gas pressure inside the bubble is relatively fixed, the curve factor decreases. The decrease of  $\kappa$  results in the development of bubbles in the  $y$  and  $z$  directions [24, 25]. This is in accordance with the energy balance of the bubble as stated by the Young-Laplace law ( $p_G = \kappa\sigma + p_L$ ), where  $\sigma$  is the surface stress,  $p_G$  is the gas pressure inside the bubble, and  $p_L$  is the liquid (water) pressure outside the bubble [6, 7, 26]. The radii of the bubble in the  $x$  axis ( $a$ , horizontal direction) are shortened. In contrast, the bubble radii of  $b$  and  $c$  (radial axis) increase because the surface stress is maximized at the terminal velocity.

During the injection, the kinetic energy of the water flow is transformed into the surface energy of the bubble and into the hydrodynamic energy of the vortex ring. These energies change the shape of the bubble from a sphere to an ellipsoidal disk, as shown in Fig. 9.

In the initial injection phase, the two-phase liquid-gas flow has an increased velocity, while the bubble diameter is not changed significantly (Fig. 10). At this condition, the momentum of the two-phase (air-water) flow is mainly used to penetrate stagnant water. Only some of the energy flow is used for the bubble change (Fig. 11,  $a$ ). If the bubble is unbalanced with respect to the surrounding environment, the bubble shape will change to follow the Young-Laplace equilibrium. The bubble shape will continually change until the terminal velocity point because of the inertial and pushing forces of the vortex ring (Fig. 11,  $b$ ). In the tail and the

nose of the bubble, there is equilibrium between the inertial and drag forces. Moreover, the ellipsoidal disk bubble is induced by the inertial force of the water flow in front of the bubble (Fig. 11,  $c$ ). The volume displacement of the water flow creates a pressure decrease in the surrounding area of the bubble nose. This is due to the surface stress energy that is transferred from the bubble edge to the bubble nose. This condition causes the drag to become lower, which causes the bubble to move in a jet flow form.

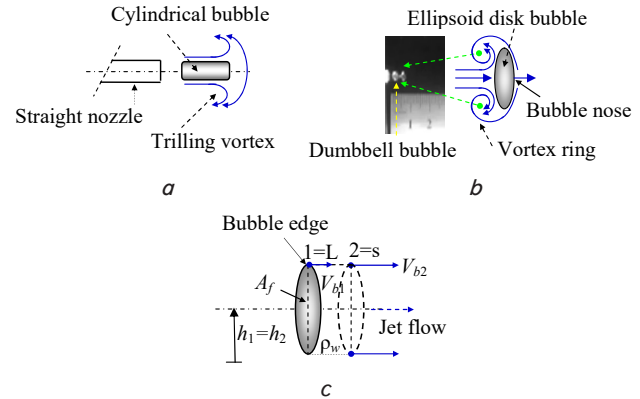


Fig. 11. Change in bubble shape:  $a$  – cylindrical bubble shape at the initial injection;  $b$  – formation of an ellipsoidal disk bubble shape owing to vortex rings;  $c$  – formation of bubble jet flow after the terminal velocity is attained

The momentum of the exiting water flow (from the bubble nose in Fig. 11,  $c$ ), is given by Bernoulli's equation in eq. (12), where the suction pressure,  $p_s$  is the local pressure of suction in front of the bubble nose,  $\rho_w$  is the water density,  $V_b$  is the bubble velocity,  $g$  is gravity, and  $h$  is the bubble level of the horizontal flow along the streamline. The water is assumed to be frictionless with a steady velocity, and incompressible flow in front of the bubble nose after the terminal velocity is followed by the moving bubble.

$$\frac{p_{1=L}}{\rho_w} + \frac{V_{b1}^2}{2} + g h_1 = \frac{p_{2=s}}{\rho_w} + \frac{V_{b2}^2}{2} + g h_2, \quad (12)$$

where 1, 2 index position;  $h_1 = h_2$  is at the horizontal flow.

$$p_L - p_s = \frac{1}{2} \rho_w (V_{b2}^2 - V_{b1}^2). \quad (13)$$

The bubble is induced by the decrease of the pressure drop around the nose. The suction pressure is attributed to the effect induced by the movement of the water flow, which leaves the bubble (Fig. 11,  $c$ ). Using a mathematical approach, the instantaneous suction pressure,  $p$ , is the water pressure minus the suction pressure ( $p = p_L - p_s$ ), as expressed by eq. (14):

$$p = \frac{1}{2} \rho_w (V_{b2}^2 - V_{b1}^2). \quad (14)$$

The size of the bubble changes owing to the decreased size of the  $a$  axis, and the increased size of the  $b$  and  $c$  axes. The size changes of the  $b$  and  $c$  axes are not as large as that for the  $a$  axis because the  $b$  and  $c$  axes are radially distributed on the frontal area of the bubble. In other words, the water flow from the straight nozzle pushes the bubble at the  $a$  axis.

As a result, it shortens the bubble size on this axis, while the bubble sizes in the *b* and *c* axes are increased radially according to square power law dependence, as indicated by (7). The change in the bubble in the *c* axis is caused by the low pressure on the bubble end-top, which is affected by the water hydrodynamic stream. A significant parameter of the bubble dynamics is the bubble shape as it is generally correlated with the physical nature of the fluid, the size, and velocity of the bubble [12]. Fig. 9 describes the change in the surface energy on the bubble. The dynamic force of the water flow pushes the bubble surface continually [25]. The deformed bubble in the flattened form is caused by the conversion of the kinetic energy to the surface energy.

The configuration of the vortex rings created by the spontaneously formed jets has been experimentally carried out with a universal time scale [27]. However, a bubble in two-phase flow was used in this study for the investigation of the changes of the bubble shape owing to the effects of vortex rings. The difference between theory and experiment indicates that there is a traveling vortex ring and vortex distortion, as also stated with the droplet breakup of a theoretical model [14]. The vortex is very strong and deforms the bubble shape, as illustrated in Fig. 11.

When the two-phase flow is injected through stagnant water, the water flow around the bubble becomes a wake flow. It creates bubbles with arbitrary shapes and tends to separate them into smaller parts. When the bubble experiences water pressure on the tail and nose, the water in front of the nose resists the moving bubble. This restricts the speed of the bubble motion, thereby deforming the bubble into an ellipsoidal disk (Fig. 11, *b*). The force of flow dynamics exerts on the working line (*x* axis) of the bubble, which is valid for analysis when using the Young-Laplace law [6, 7]. An increase in the gas pressure coincides with a decrease of the surface tension. Meanwhile, the surface tension in the edge part of the ellipsoidal disk will increase. The edge surface tension reaches a maximum value at equilibrium between the inertial force and the drag force or occurs when the terminal velocity point is reached. The availability of the second velocity around the bubble nose causes the water pressure to decrease. The bubble is then conditioned toward the Young-Laplace equilibrium [6]. The surface tension of the bubble-end leads to a new Young-Laplace balance in all the surfaces, which is appropriate given the bubble surroundings. This balanced condition is followed by the shape deformation toward the theoretically predicted spherical shape. The deformation associated with the shape change from an ellipsoidal disk to a sphere will be decreased by the drag. In addition, if the drag on the bubble nose decreases, the equilibrium between the inertial and drag forces is disturbed. Therefore, the bubble flows again following a sudden velocity increase.

The velocity increase of the flow injection cannot break up a bubble if the energy density of the bubble surface is higher than that of the water flow. A slight decrease of the velocity during the movement of the bubble from one position to the next is often expressed as velocity turning (or turning angle  $\theta$ ), as illustrated in Fig. 12, *a*. The shape change of the bubble follows the Young-Laplace law, which is balanced by its surrounding pressure (Fig. 12, *b*). The shear fields change the bubble shape, which causes the frontal area of the bubble to increase [28]. This change decreases the bubble velocity. Accordingly, the maximum frontal area occurs at the terminal velocity point (Fig. 12, *c*). The

frontal area is the barrier of the flow field in the two-phase flow. A bubble will experience an increase in the flow-field barrier when it is injected into the fluid. The behavior of a single bubble can thus represent the behavior of a number of bubbles contained in the two-phase flow injection. It is considered that the bubble decreases the velocity of the water flow and affects the decrease of the centrifugal force when it occurs in the cyclonic separator [29]. Other examples can be found in the charge lines of automotive vehicles in which the bubbles can affect the discontinuity supply of the charge.

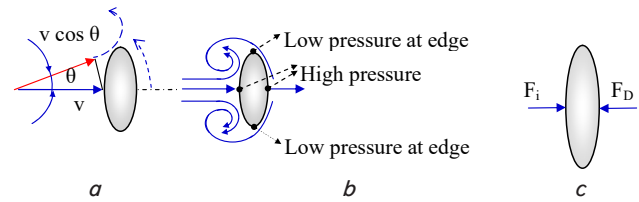


Fig. 12. Hydrodynamic effects around the bubble:  
*a* – velocity turning with angle  $\theta$  owing to the bubble profile;  
*b* – pressure condition of bubble surroundings;  
*c* – terminal velocity point achieved upon force balance

It is difficult to measure the magnitudes of the vortices that restrict the water flow in the two-phase flow injection in the motionless water. However, this can be solved by observing the bubble shape changes within the flow field [30]. An increase in the bubble size due to a change in height (in the *z*-axis) decreases the length (in the *x*-axis) of the bubble. This leads to changes of the drag area in the frontal area. In Fig. 10, it was indicated that there is a significant difference between experiment and theory, whereby the magnitude of the vortex influences the bubble shape in addition to the influences of the inertia of the water flow. The largest changes occurred at the point of terminal velocity. Accordingly, eq. (1) becomes:

$$F_i + F_T = F_v + F_D. \tag{15}$$

When the bubble exits the nozzle, the inertial force of water gradually decreases, while the vortex force,  $F_T$  gradually increases, as stated by eq. (15). Conversely, from the outlet nozzle to the terminal velocity point (Fig. 12, *c*), the drag force increases. Meanwhile, a very small viscous force will disappear or reach a zero value [6, 12]. Restriction on the two-phase flow of the solid material does not change, while the restriction on the two-phase flow of the bubble gas increases and achieves the maximum value when the terminal velocity condition is reached.

## 7. Conclusions

1. The growth of bubbles in theory and experiment has a difference. This is influenced by the presence of hydrodynamic flow, which plays a role in changing the shape of bubbles. The continuous flow of water presses on the bubble tail and is held by stagnant water on the bubble nose, so the bubbles change radially at the frontal area. This area is then matched to the frontal area based on the bubble height in the experiment. The results show the same trend.

2. Changes in the frontal area of the bubble that continues to increase then after the terminal velocity point has decreased, this shows the existence of a maximum frontal

area. The change in the frontal area between theory and experiment is significant at the terminal velocity point. This shows that there is the biggest flow resistance.

3. The bubble size in the experiment is significantly greater than in theory. This shows the existence of hydro-

dynamic flow, which increases the frontal area of the bubble. So the drag flow increases, which affects the decrease in centrifugal force. This force plays a role in the gas-water separation process. This problem indicates that the results of the separation are not satisfactory.

## References

1. Chu, P., Waters, K. E., Finch, J. A. (2016). Break-up in formation of small bubbles: Break-up in a confined volume. *Colloids and Surfaces A: Physicochemical and Engineering Aspects*, 503, 88–93. doi: <https://doi.org/10.1016/j.colsurfa.2016.05.037>
2. Movafaghian, S., Jaua-Marturet, J. A., Mohan, R. S., Shoham, O., Kouba, G. E. (2000). The effects of geometry, fluid properties and pressure on the hydrodynamics of gas–liquid cylindrical cyclone separators. *International Journal of Multiphase Flow*, 26 (6), 999–1018. doi: [https://doi.org/10.1016/s0301-9322\(99\)00076-2](https://doi.org/10.1016/s0301-9322(99)00076-2)
3. Rosa, E. S., França, F. A., Ribeiro, G. S. (2001). The cyclone gas–liquid separator: operation and mechanistic modeling. *Journal of Petroleum Science and Engineering*, 32 (2-4), 87–101. doi: [https://doi.org/10.1016/s0920-4105\(01\)00152-8](https://doi.org/10.1016/s0920-4105(01)00152-8)
4. Bozzano, G., Dente, M. (2001). Shape and terminal velocity of single bubble motion: a novel approach. *Computers & Chemical Engineering*, 25 (4-6), 571–576. doi: [https://doi.org/10.1016/s0098-1354\(01\)00636-6](https://doi.org/10.1016/s0098-1354(01)00636-6)
5. Emami, A., Briens, C. (2008). Study of downward gas jets into a liquid. *AIChE Journal*, 54 (9), 2269–2280. doi: <https://doi.org/10.1002/aic.11524>
6. Tomiyama, A., Celata, G. P., Hosokawa, S., Yoshida, S. (2002). Terminal velocity of single bubbles in surface tension force dominant regime. *International Journal of Multiphase Flow*, 28 (9), 1497–1519. doi: [https://doi.org/10.1016/s0301-9322\(02\)00032-0](https://doi.org/10.1016/s0301-9322(02)00032-0)
7. Bari, S. D., Robinson, A. J. (2013). Experimental study of gas injected bubble growth from submerged orifices. *Experimental Thermal and Fluid Science*, 44, 124–137. doi: <https://doi.org/10.1016/j.expthermflusci.2012.06.005>
8. Rassame, S., Hibiki, T., Ishii, M. (2016). Void penetration length from air injection through a downward large diameter submerged pipe in water pool. *Annals of Nuclear Energy*, 94, 832–840. doi: <https://doi.org/10.1016/j.anucene.2016.04.046>
9. Bai, H., Thomas, B. G. (2001). Bubble formation during horizontal gas injection into downward-flowing liquid. *Metallurgical and Materials Transactions B*, 32 (6), 1143–1159. doi: <https://doi.org/10.1007/s11663-001-0102-y>
10. Mandal, A. (2010). Characterization of gas-liquid parameters in a down-flow jet loop bubble column. *Brazilian Journal of Chemical Engineering*, 27 (2), 253–264. doi: <https://doi.org/10.1590/s0104-66322010000200004>
11. Liu, Z., Reitz, R. D. (1997). An analysis of the distortion and breakup mechanisms of high speed liquid drops. *International Journal of Multiphase Flow*, 23 (4), 631–650. doi: [https://doi.org/10.1016/s0301-9322\(96\)00086-9](https://doi.org/10.1016/s0301-9322(96)00086-9)
12. Liu, L., Yan, H., Zhao, G. (2015). Experimental studies on the shape and motion of air bubbles in viscous liquids. *Experimental Thermal and Fluid Science*, 62, 109–121. doi: <https://doi.org/10.1016/j.expthermflusci.2014.11.018>
13. Hinze, J. O. (1955). Fundamentals of the hydrodynamic mechanism of splitting in dispersion processes. *AIChE Journal*, 1 (3), 289–295. doi: <https://doi.org/10.1002/aic.690010303>
14. Han, L., Luo, H., Liu, Y. (2011). A theoretical model for droplet breakup in turbulent dispersions. *Chemical Engineering Science*, 66 (4), 766–776. doi: <https://doi.org/10.1016/j.ces.2010.11.041>
15. Cihonski, A. J., Finn, J. R., Apte, S. V. (2013). Volume displacement effects during bubble entrainment in a travelling vortex ring. *Journal of Fluid Mechanics*, 721, 225–267. doi: <https://doi.org/10.1017/jfm.2013.32>
16. Gao, L., Yu, S. C. M. (2010). A model for the pinch-off process of the leading vortex ring in a starting jet. *Journal of Fluid Mechanics*, 656, 205–222. doi: <https://doi.org/10.1017/s0022112010001138>
17. Jiang, X. F., Zhu, C., Li, H. Z. (2017). Bubble pinch-off in Newtonian and non-Newtonian fluids. *Chemical Engineering Science*, 170, 98–104. doi: <https://doi.org/10.1016/j.ces.2016.12.057>
18. Tomiyama, A., Kataoka, I., Zun, I., Sakaguchi, T. (1998). Drag Coefficients of Single Bubbles under Normal and Micro Gravity Conditions. *JSME International Journal Series B*, 41 (2), 472–479. doi: <https://doi.org/10.1299/jsmeb.41.472>
19. Vincent, F., Le Goff, A., Lagubeau, G., Quéré, D. (2007). Bouncing Bubbles. *The Journal of Adhesion*, 83 (10), 897–906. doi: <https://doi.org/10.1080/00218460701699765>
20. Walter, J. F., Blanch, H. W. (1986). Bubble break-up in gas – liquid bioreactors: Break-up in turbulent flows. *The Chemical Engineering Journal*, 32 (1), B7–B17. doi: [https://doi.org/10.1016/0300-9467\(86\)85011-0](https://doi.org/10.1016/0300-9467(86)85011-0)
21. Moore, D. W. (1965). The velocity of rise of distorted gas bubbles in a liquid of small viscosity. *Journal of Fluid Mechanics*, 23 (4), 749–766. doi: <https://doi.org/10.1017/s0022112065001660>
22. Aoyama, S., Hayashi, K., Hosokawa, S., Tomiyama, A. (2016). Shapes of ellipsoidal bubbles in infinite stagnant liquids. *International Journal of Multiphase Flow*, 79, 23–30. doi: <https://doi.org/10.1016/j.ijmultiphaseflow.2015.10.003>
23. Hreiz, R., Lainé, R., Wu, J., Lemaitre, C., Gentric, C., Fünfschilling, D. (2014). On the effect of the nozzle design on the performances of gas–liquid cylindrical cyclone separators. *International Journal of Multiphase Flow*, 58, 15–26. doi: <https://doi.org/10.1016/j.ijmultiphaseflow.2013.08.006>
24. Tomita, Y., Robinson, P. B., Tong, R. P., Blake, J. R. (2002). Growth and collapse of cavitation bubbles near a curved rigid boundary. *Journal of Fluid Mechanics*, 466, 259–283. doi: <https://doi.org/10.1017/s0022112002001209>
25. Fei, Y., Pang, M. (2019). A treatment for contaminated interfaces and its application to study the hydrodynamics of a spherical bubble contaminated by surfactants. *Chemical Engineering Science*, 200, 87–102. doi: <https://doi.org/10.1016/j.ces.2019.01.052>

26. Chen, Y., Groll, M. (2006). Dynamics and shape of bubbles on heating surfaces: A simulation study. *International Journal of Heat and Mass Transfer*, 49 (5-6), 1115–1128. doi: <https://doi.org/10.1016/j.ijheatmasstransfer.2005.07.053>
27. Gharib, M., Rambod, E., Shariff, K. (1998). A universal time scale for vortex ring formation. *Journal of Fluid Mechanics*, 360, 121–140. doi: <https://doi.org/10.1017/s0022112097008410>
28. Canedo, E. L., Favelukis, M., Tadmor, Z., Talmon, Y. (1993). An experimental study of bubble deformation in viscous liquids in simple shear flow. *AIChE Journal*, 39 (4), 553–559. doi: <https://doi.org/10.1002/aic.690390403>
29. Uchiyama, T., Sasaki, S. (2014). Experimental Investigation of the Interaction between Rising Bubbles and Swirling Water Flow. *International Journal of Chemical Engineering*, 2014, 1–10. doi: <https://doi.org/10.1155/2014/358241>
30. Yuan, D., Xiao, Z., Chen, D., Zhong, Y., Yan, X., Xu, J., Huang, Y. (2016). Numerical Investigation on Bubble Growth and Sliding Process of Subcooled Flow Boiling in Narrow Rectangular Channel. *Science and Technology of Nuclear Installations*, 2016, 1–12. doi: <https://doi.org/10.1155/2016/7253907>

У даній роботі викладені методи структурно-параметричного синтезу і кінематичного аналізу паралельного маніпулятора з трьома ступенями свободи, що працює в циліндричній системі координат. Цей паралельний маніпулятор відноситься до класу RoboMech, оскільки він працює за заданими законами рухів робочого органу і приводів, що спрощує систему управління і покращує її динаміку. Паралельні маніпулятори класу RoboMech працюють з певними структурними схемами і геометричними параметрами їх ланок. Розглянутий паралельний маніпулятор формується шляхом з'єднання вихідної точки з основою з використанням однієї пасивної і двох активних замикаючих кінематичних ланцюгів (ЗКЛ). Пасивний ЗКЛ має нульову ступінь свободи і він не накладає геометричний зв'язок на рух вихідної точки, тому геометричні параметри ланок пасивного ЗКЛ вільно варіюються. Активні ЗКЛ мають активні кінематичні пари і вони накладають геометричні зв'язки на рух вихідної точки. Геометричні параметри ланок активних ЗКЛ визначаються на основі апроксимаційних задач Чебишевського і квадратичного наближень. Для цього складено рівняння геометричних зв'язків у вигляді функцій зважених різниць, які представлені у вигляді узагальнених (Чебишевських) поліномів. Це призводить до лінійних ітераційних задач.

Вирішені пряма і зворотна задачі кінематики досліджуваного паралельного маніпулятора. У прямій задачі кінематики за заданими положеннями вхідних ланок визначені координати вихідної точки. У зворотній задачі кінематики за координатами вихідної точки визначаються положення вхідних ланок. Пряма і зворотна задачі кінематики досліджуваного паралельного маніпулятора зводяться до рішень задач про положення діад Сильвестра. Представлені чисельні результати структурно-параметричного синтезу і кінематичного аналізу розглянутого паралельного маніпулятора. Чисельні результати кінематичного аналізу показують, що максимальне відхилення руху вихідної точки від ортогональних траєкторій становить 1,65 %

**Ключові слова:** паралельний маніпулятор, RoboMech, циліндричні системи координат, Чебишевське і квадратичне наближення

UDC 621.01

DOI: 10.15587/1729-4061.2020.203131

## A ROBOMECH CLASS PARALLEL MANIPULATOR WITH THREE DEGREES OF FREEDOM

**Zh. Baigunchekov**

Director

Scientific and Educational Centre of Digital Technologies and Robotics\*

Professor

Department of Mechanical Engineering\*\*

**A. Mustafa**

Doctoral Student

Institute of Industrial Engineering\*\*

E-mail: mustafa\_azamat@mail.ru

**T. Sobh**

Professor\*\*\*

**S. Patel**

Professor\*\*\*

**M. Utenov**

Professor\*

\*Al-Farabi Kazakh National University

al-Farabi ave., 71, Almaty,

Republic of Kazakhstan, 050040

\*\*Satbayev University

Satpaev str., 22a, Almaty, Republic of Kazakhstan, 050013

\*\*\*University of Bridgeport

Park ave., 126, Bridgeport, CT 06604,

United States of America

Received date 25.03.2020

Accepted date 11.05.2020

Published date 19.06.2020

Copyright © 2020, Zh. Baigunchekov, A. Mustafa, T. Sobh, S. Patel, M. Utenov

This is an open access article under the CC BY license

(<http://creativecommons.org/licenses/by/4.0>)

### 1. Introduction

Existing methods of designing both serial and parallel manipulating robots are mainly reduced to solving the inverse kinematics problem, i. e. determining the laws of

movements of manipulator actuators according to the specified laws of movements of end-effectors, followed by the development of control systems. At the same time, manipulator actuators usually operate in controlled modes of intensive accelerations and decelerations, which worsens their dynamics and reduces efficiency.